



## Floating marine debris surface drift: Convergence and accumulation toward the South Pacific subtropical gyre

Elodie Martinez<sup>a,b,\*</sup>, Keitapu Maamaatuaiahutapu<sup>a</sup>, Vincent Taillandier<sup>b</sup>

<sup>a</sup>Laboratoire Terre-Océan, Université de la Polynésie Française, BP 6570 Faaa, Faaa 98702, Tahiti French Polynesia, France

<sup>b</sup>Laboratoire d'Océanographie de Villefranche (LOV), CNRS UMR 7093, Université Pierre et Marie Curie, BP 08, 06 238 Villefranche sur Mer, France

### ARTICLE INFO

#### Keywords:

Surface currents  
Satellite data  
Lagrangian drift  
Floating marine debris  
Convergence zone  
Accumulation area

### ABSTRACT

Whatever its origin is, a floating particle at the sea surface is advected by ocean currents. Surface currents could be derived from *in situ* observations or combined with satellite data. For a better resolution in time and space, we use satellite-derived sea-surface height and wind stress fields with a  $1/3^\circ$  grid from 1993 to 2001 to determine the surface circulation of the South Pacific Ocean. Surface currents are then used to compute the Lagrangian trajectories of floating debris. Results show an accumulation of the debris in the eastern-centre region of the South Pacific subtropical gyre ( $[120^\circ\text{W}; 80^\circ\text{W}]$ – $[20^\circ\text{S}; 40^\circ\text{S}]$ ), resulting from a three-step process: in the first two years, mostly forced by Ekman drift, the debris drift towards the tropical convergence zone ( $\sim 30^\circ\text{S}$ ). Then they are advected eastward mostly forced by geostrophic currents. They finally reach the eastern-centre region of the South Pacific subtropical gyre from where they could not escape.

© 2009 Elsevier Ltd. All rights reserved.

### 1. Introduction

Floating marine debris (FMD) and other marine pollution threaten the livelihood of coastal communities. Coastlines are strewn with a myriad of light-weight plastic bags and other debris, mar- rying the paradise image of the South Pacific, endangering shipping and human health as well as threatening marine life. It is estimated that each year around the world more than 100,000 sea animals, including turtles, die from eating or being caught in plastic bags and other debris (Wilks, 2006). Despite control measures, the amount of litter at sea is increasing (Ryan and Moloney, 1993) and the predominance of plastics varies between 60% and 80% of the total marine debris (Gregory and Ryan, 1997). Their durability in the marine environment is still uncertain but they seem to last from 3 to 10 years, and additives can probably extend this period to 30–50 years (Gregory, 1978).

Transport of particles by ocean currents is important in physical oceanography since the particles can be used as a tracer of the ocean circulation. Conversely, our knowledge of the ocean currents could help us find the trajectories of FMD in order to study pollut- ing FMD (Kubota et al., 2005) or to study invasive species (Martinez et al., 2007). On a large scale, extensive studies of FMD have been carried out in the North Pacific Ocean. Wakata and Sugimori

(1990) investigated surface drift simulations using ship drift data. Three high-density accumulation areas exist and one of these stag- nates north of the Hawaii islands. The accumulation mechanism in this area was clarified by Kubota (1994), using surface currents cal- culated by combining Ekman and Stokes drifts and geostrophic currents. Stokes and Ekman drifts were derived from COADS ocean wind data, while geostrophic currents were derived from Levitus salinity and temperature data. Then Kubota et al. (2005), used monthly ERS winds and 5-day Topex/Poseidon sea surface height on a  $1^\circ$  grid in order to calculate surface current fields for the world ocean from 1993 to 1998. The Stokes drift effect on the motion of FMD was considered to be less significant than geostrophic cur- rents and Ekman drifts. Focusing on the North Pacific, the authors showed that after a five-year drift FMD accumulate in specific high density areas such as the mid latitudes and north of Hawaii. A sim- ilar trend of mid-latitude convergence in other ocean basins as well as in the South Pacific Ocean has been reported by Kubota et al. (2005).

The present work is intended to characterize and quantify long- term drift of FMD in the South Pacific Ocean. This oceanic basin is insufficiently sampled by surface drifters, especially in its central part, to provide a suitable spatial coverage. Moreover, drifters al- most never start their drifts from coasts but in the open ocean and they could not operate longer than three years. For our pur- pose, satellite data are more suitable mostly with the unprece- dented  $1/3^\circ$ -spatial and 7-day temporal global coverage from 1993 to 2001. Considering the durability of FMD (10 years or more), it is possible with this data set to explore the long-term drift

\* Corresponding author. Address: Laboratoire d'Océanographie de Villefranche (LOV), CNRS UMR 7093, Université Pierre et Marie Curie, BP 08, 06 238 Villefranche- sur-Mer, France. Tel.: +33 4 93 76 37 23; fax: +33 4 93 76 37 39.

E-mail address: [martinez@obs-vlfr.fr](mailto:martinez@obs-vlfr.fr) (E. Martinez).

of FMD in the South Pacific Ocean and to answer the question about the FMD fate after they reach the convergence region in the mid latitudes. Assessment of the impact of interannual variability due to ENSO (El Niño Southern Oscillation) is carried out. Our data set allows us to explore the effect of mesoscale structures on FMD drift. Such higher spatial resolution data set is particularly useful in the South Pacific mid latitudes where the SubTropical CounterCurrent (STCC) flows. The STCC is highly turbulent (Qiu and Chen, 2004) and should impact on drift trajectories.

This paper is organized as follows: in Section 2 data and processing procedures are presented. In Section 3, Lagrangian trajectories and trends in the South Pacific Ocean are identified. Comparisons with results calculated from the OSCAR (Ocean Surface Current Analysis-Real time) product are carried out. A summary and discussion are provided in Section 4.

## 2. Data and methods

### 2.1. Satellite derived high spatial resolution sea surface currents

Surface oceanic currents are calculated from sea level anomaly (SLA) and sea surface wind satellite data products from January 1993 to January 2001 in the South Pacific Ocean ( $[5^{\circ}\text{N}; 60.5^{\circ}\text{S}]$  and  $[139.5^{\circ}\text{E}; 70.5^{\circ}\text{W}]$ ). SLA data are extracted weekly from the combined TOPEX/POSEIDON (T/P) (Fu et al., 1994; Stammer and Wunch, 1994) and ERS-1/2 (Ducet and Le Traon, 2001) data on a  $1/3^{\circ}$  grid. SLA data are added to the Levitus mean annual climatological dynamic height referred to 1000 m depth (Levitus et al., 1992) to calculate the surface geostrophic currents. Geostrophy is established from the standard  $f$ -plane geostrophic balance with a special attention near the equator where the coriolis parameter is equal to zero. As in the method presented by Lagerloef et al. (1999), geostrophy varies smoothly from a  $\beta$ -plane formulation at the equator to an  $f$ -plane formulation at mid latitude, with the transition occurring at  $\sim 2^{\circ}$ – $3^{\circ}$  latitude. The transition is interpolated with Gaussian weighted functions.

The Ekman current is calculated from a parametric model of the purely wind-driven response (Pond and Pickard, 1983). About 10 m-high wind fields are measured by the ERS-1/2 scatterometers and provided by PODAAC (Physical Oceanography distributed Active Archive Center). Wind fields are linearly, temporally and spatially interpolated to fit the 7-day interval,  $1/3^{\circ}$  gridded field of T/P-ERS SLA from January 1993 to January 2001. At the equator, Ekman current vectors are considered as 3% of the wind vectors to make a smooth transition with conventional wind currents calculated for higher latitudes (Chen et al., 1999; Lagerloef et al., 1999).

Surface circulation features in the South Pacific Ocean are described with a good resolution (Le Traon et al., 2003) from 1993 to 2001, every 7 days on a Mercator  $1/3^{\circ}$  grid as the sum of geostrophic and Ekman currents, and will be referred as the *High Resolution (HR)* total, geostrophic and Ekman fields.

### 2.2. HR mesoscale filtered field

A degraded version of HR field is also used in this study to investigate the sensitivity to mesoscale current structures. The mesoscale patterns are filtered out from the original HR fields. Keeping the same meshgrid, the mesoscale filter has consisted in applying a moving spatial average over a radius equal to 200 km.

### 2.3. OSCAR sea surface currents

The OSCAR sea surface currents are provided by NOAA (<http://www.oscar.noaa.gov>), on a  $1^{\circ}$  resolution grid, weekly from 1993 to 2001. This product is constructed from the TOPEX/Poseidon

sea surface heights, scatterometer winds, and both Advanced Very High Resolution Radiometer and *in situ* sea surface temperatures (Bonjean and Lagerloef, 2002). It is representative of the surface layer (upper 30 m depth).

With a  $1^{\circ}$  spatial resolution, OSCAR surface currents will be referred as the *Low Resolution (LR)* product compared to the HR product presented in Section 2.1.

### 2.4. Eddy kinetic energy

The weekly Eddy kinetic energy is calculated using altimetry data (Jakobsen et al., 2003; Martins et al., 2002; Ducet and Le Traon, 2001):  $EKE = 1/2[(u_g')^2 + (v_g')^2]$ , where  $u_g'$  and  $v_g'$ , respectively, are the zonal and meridian components of the geostrophic anomaly field. This anomaly field is obtained removing the 8 year (1993–2001) average to the weekly geostrophic fields.

### 2.5. The Lagrangian drift

FMD are assumed to be transported by the sea surface currents derived from satellite data (Sections 2.1–2.3). Their trajectories are then represented by the successive positions  $r = (\lambda, \varphi)$  that FMD cross by during the 8 years period of interest (1993–2001) inside the Southern Pacific Ocean.

In numerical practice, the advection of a passive particle inside a 2D velocity field can be described by a solution of the non-linear ordinary equation  $\frac{dr}{dt} = \mathbf{u}(r, t)$ , with the initial condition  $r(t_0)$ . This equation is classically and accurately resolved using the 4th order Runge–Kutta scheme for the integration of the time derivation, and a bilinear interpolation in space for the velocity term  $\mathbf{u}(r, t)$ .

Its discrete formulation requires the specification of a time step which duration is to be consistent with the spatial resolution of the velocity field. Given a  $1/3^{\circ}$  resolution at most for the ocean surface currents data, the time step is fixed at 1 day in order to account for the local velocity structures along the FMD motion. With an average motion of 20 km per day, the FMD trajectory would be sampled in each mesh of the velocity field and so forced by all the surrounding velocity values (see Taillandier et al., 2006 for detailed discussion).

The FMD are represented by a large population of numerical particles that are homogeneously distributed at the initial time of the experiment. The distribution of this population over the South Pacific Ocean is computed weekly but the outputs are considered with a periodicity of a month. Each month, the number of numerical particles is computed inside each  $1^{\circ} \times 1^{\circ}$  bin covering the whole basin. The number of numerical particles which have not moved during this 1 month period is also performed to quantify a rate of disappearance of the population. This distribution at the initial and final times is also extracted for each simulation.

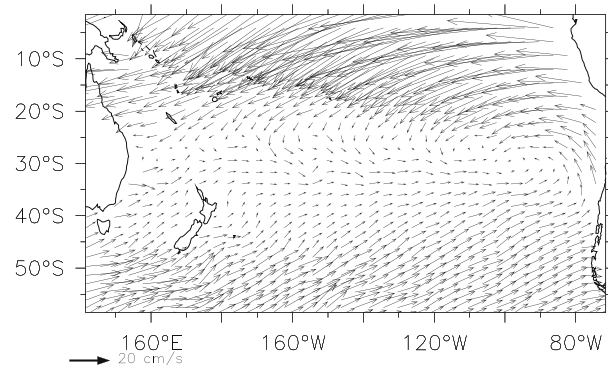


Fig. 1. Mean surface current from January 1993 to January 2001.

A series of 6 numerical experiments is performed using this method and providing this diagnostic. The first experiment involves the *HR total* velocity fields, as presented in Section 2.1, describing sea surface currents. The second experiment only uses *HR Ekman* related ocean surface currents. The third experiment only uses *HR geostrophic* relative ocean surface currents. The fourth experiment uses *LR OSCAR* currents as described in Section 2.3. The fifth experiment uses the *spatially filtered HR total* velocity fields (Section 2.2). These five experiments are carried out over the 8-year period. In addition, a series of 2 year experiments are considered with the *HR total* currents in order to investigate *inter annual variability*. The time of the initial condition is then set to be the first day of each year from 1993 to 1999.

### 3. Drift trajectories in the South Pacific

#### 3.1. The South Pacific mean surface currents

The mean surface oceanic circulation, calculated from 1993 to 2001, shows the well-documented anticyclonic circulation around the subtropical gyre of the South Pacific Ocean (Fig. 1).

At the northern boundary, the South Equatorial Current (SEC) flows southwestward with the highest surface velocities close to the equator (about 40–50 cm/s), as reported by Jingzhi et al. (2006) using drifter data archived in the Marine Environmental Data Service (MEDS). The mean velocity of the surface SEC decreases farther south and reaches about 10–20 cm/s around 20°S. On the western boundary, along the Australian coast, the flow turns southward in the highly turbulent East Australian Current (EAC) with 40 cm/s mean velocity from 27°S to 35°S and up to 60 cm/s. This is consistent with the 60 cm/s velocity along 30°S and until 40 km from the coast found by Mata et al. (2000). Around 35°S, the eastward South Pacific Current (SPC) crosses the ocean with less than 10 cm/s velocity as found by Stamma et al. (1995). South of 45°S, the Antarctic Circumpolar Current (ACC) crosses the basin eastward and leaves the South Pacific basin via the Drake Passage. Its velocities are less than 20 cm/s but larger in fronts although ACC transports more water than any other current (Klinck and Nowlin, 2001). On the eastern boundary, the Peru/Chile Current can be detected at 40°S. The northward velocity of this current reaches up to 15 cm/s near the coast, and decreases to 5 cm/s

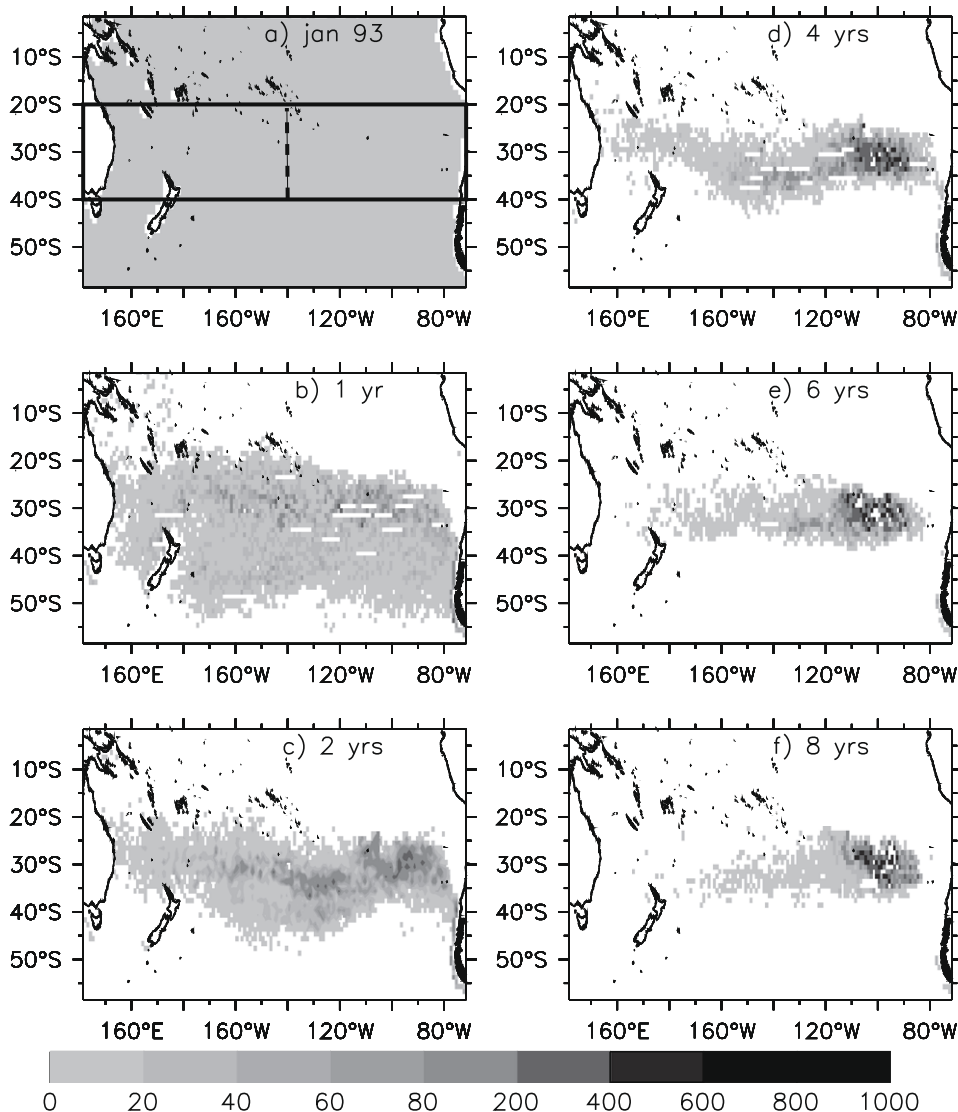


**Fig. 2.** FMD spatial distribution averaged on a 1° resolution grid. (a) Initial time, (b) after 1 year, (c) after 2 years, (d) after 4 years, (e) after 6 years and (f) after 8 years. On (a) is plotted the box corresponding to the convergence zone ([150°E; 70°W] & [20°S; 40°S]). It is divided (dashed line) in two regions: its western part ([150°E; 140°W] & [20°S; 40°S]), and its eastern part ([140°W; 70°W] & [20°S; 40°S]), i.e. the accumulation area.

west of the coast consistently with [Jingzhi et al. \(2006\)](#) and [Chaigneau and Pizarro \(2005\)](#) who used satellite-tracked drifters.

3.2. FMD drift derived from the HR surface currents

[Fig. 2](#) summarizes the particle drifts from January 1993 to January 2001 using the HR total surface current field. The simulation is initiated with a sampling on a  $1/3^\circ$  grid ([Fig. 2a](#)) corresponding to a total amount of 84,522 particles. After one year ([Fig. 2b](#)), about 18% of the particles run aground on coasts or leave the South Pacific Ocean through the Coral Sea, the Drake Passage and along the equator. The amount of particles leaving the South Pacific Ocean rises to 24% after two years of drift and hardly changes the next 6 years (26% after 8 years of drift). About 75% of the total amount of 84,522 particles flow into the South Pacific Ocean.

[Figs. 2c and 3a](#) (thick line) show that after two years, 95% of the 75% remaining FMD gather in the convergence zone [ $150^\circ\text{E}-70^\circ\text{W}$ ] and [ $20^\circ\text{S}-40^\circ\text{S}$ ] (as plotted in [Fig. 2a](#)). The fast drift of FMD towards the convergence zone is due to the strong meridian component of the current north  $15^\circ\text{S}$  and south  $45^\circ\text{S}$  as it is shown in [Fig. 1](#). In the western part of the convergence zone [ $150^\circ\text{E}-140^\circ\text{W}$ ;  $20^\circ\text{S}-40^\circ\text{S}$ ] (plotted in [Fig. 2a](#)), the FMD density as shown in [Fig. 3b](#) increases to 35% after one year and then decreases to 0% as the particles are transported eastward. In the eastern part of the

convergence zone [ $140^\circ\text{W}-70^\circ\text{W}$ ;  $20^\circ\text{S}-40^\circ\text{S}$ ], the FMD density increases to 100% after 8 years drift ([Figs. 2f and 3c](#)).

The spatial distribution of the debris ([Fig. 2](#)) shows that they are quickly confined in the convergence zone. After eight years of drift, FMD are mostly found in the eastern-centre region of the subtropical gyre between [ $140^\circ\text{W}-70^\circ\text{W}$ ] and [ $20^\circ\text{S}-40^\circ\text{S}$ ] ([Fig. 2f](#)). FMD are trapped in this region, the accumulation zone, from where they cannot escape. Complementary simulations have been carried out with an initial sampling every  $0.2^\circ$  on several  $5^\circ$  by  $5^\circ$  areas in the accumulation zone. Our results confirm that during the eight year drift of FMD, none escapes from the accumulation zone.

The surface currents used in this Section 3.2 have combined geostrophic and Ekman components. In Section 3.3, we investigate the drift characteristics provided by the HR Ekman to geostrophic fields separately.

3.3. Induced HR Ekman and geostrophic drifts

As we mentioned in Section 3.2, the rapid drift of FMD towards the convergence zone between  $20^\circ\text{S}$  and  $40^\circ\text{S}$  that occurs in the first two years is mainly due to the Ekman drift ([Fig. 3a](#), thick dashed line) in agreement with the strong meridian component of the mean surface current north of  $15^\circ\text{S}$  and south of  $45^\circ\text{S}$  ([Fig. 1](#)). The Ekman current plays a dominant role in maintaining FMD in the convergence zone. This result is in agreement with observations reported by [Maximenko \(2006\)](#). In the western part of the convergence zone ([Fig. 3b](#)), the FMD density increases to reach a maximum value of 48% after two years simulation. The FMD density is maintained above 40% by the Ekman drift for the rest of the time. Similar observations are found for the eastern part of the convergence zone.

FMD drift deduced from the geostrophic currents alone differs from the drift calculated from the Ekman current alone. The FMD density in the convergence zone slightly decreases from 35% to 25% ([Fig. 3a](#), thick dotted line). The role played by the geostrophic

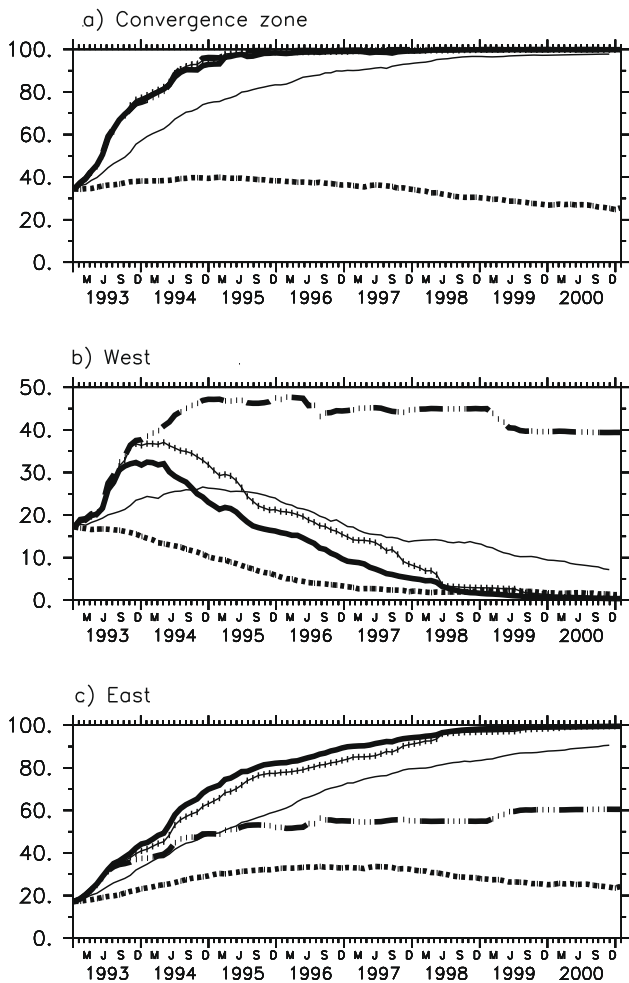


**Fig. 3.** Density (in%) of drifting marine debris present in: (a) the convergence zone, (b) its western part and (c) its eastern part; from the surface HR total current (thick solid line), HR geostrophic current (thick dotted line), HR Ekman current (thick dashed line), HR mesoscale filtered total current (thin line with vertical bars), and LR OSCAR total current (thin line).

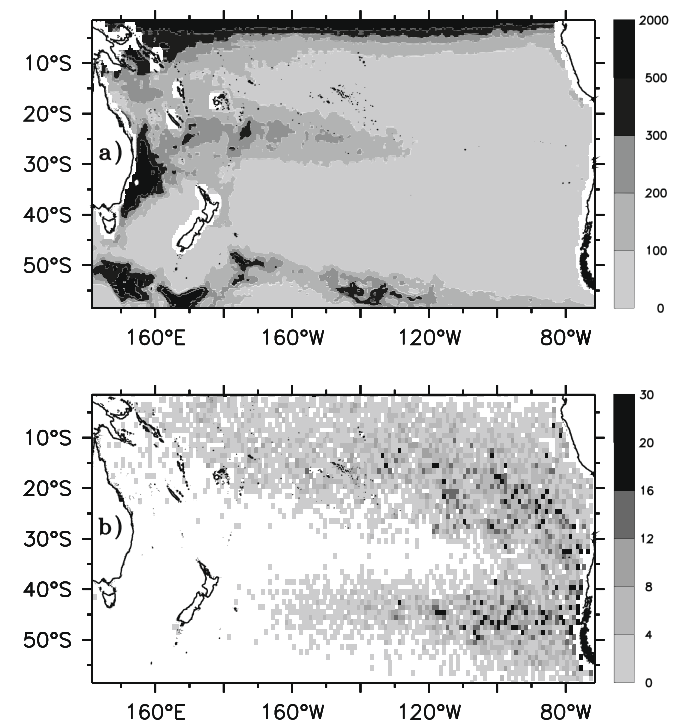


**Fig. 4.** (a) Mean annual EKE ( $\text{cm}^2/\text{s}^2$ ) calculated from TP/ERS SLA, from 1993 to 2001, and (b) particle position after an eight year drift following the  $1/3^\circ$  high resolution geostrophic surface current derived from TP/ERS SLA.

current is better observed when analyzing sub-regions of the convergence zone. In the eastern part of the convergence zone, the geostrophic currents maintain the FMD density at a level of 20% during the eight years simulation. In the western part of the convergence zone, the FMD density decreases from 18% to less than 5% in about four years showing that the geostrophic currents transport particles toward the eastern region. To confirm this mechanism and to determine which currents are at the origin of this eastward transport, the mean annual Eddy kinetic energy (EKE) derived from TP/ERS SLA has been computed and compared to the spatial distribution of FMD after an eight years simulation (Fig. 4). The most energetic area is located along the western boundary of the oceanic basin, in the EAC from 25°S to 40°S. For our purpose, the most interesting area is the [20–30°S; 167–135°W] band where the weak and turbulent SubTropical Counter-Current (STCC) flows eastward (Qiu and Chen, 2004; Morris et al., 1996; Merle et al., 1969s) with a strong EKE (from 100 to 300 m<sup>2</sup>/s<sup>2</sup>). The simulation based on the geostrophic field alone shows that FMD are transported away from the western part of the convergence zone by the STCC (Fig. 4). Fig. 4b shows that high FMD densities are found in the eastern part of the South Pacific Ocean out of the high EKE areas. However, FMD are not confined in the eastern part of the convergence zone as shown in Fig. 2.

At the scale of the South Pacific Ocean basin, the basic mechanisms of the FMD drift consists in a three-step process: first, FMD converge to the tropical convergence zone due to the wind induced Ekman drift; second, they are transported eastward by geostrophic currents; third, FMD are maintained by the Ekman currents in the eastern part of the convergence zone.

#### 3.4. Comparison with the LR OSCAR surface current field and the HR mesoscale filtered field

Transport of FMD by surface currents from our HR simulation with both the LR OSCAR and the HR mesoscale filtered simulations are compared. The same large scale trends in drift trajectories are found: convergence – eastward drift – accumulation.

However, to achieve the same FMD density level in the convergence zone as in the HR simulation model, a longer period of time is required in the LR simulation model (Fig. 3a, thin line). One more year is necessary in the LR simulation to reach a maximum density in the western region of the convergence zone (Fig. 3b). FMD are kept longer in the western part of the convergence zone in the LR simulation. The difference between HR and LR densities in the eastern region increases and remains constant after three years (Fig. 3c). The discrepancies could be explained by our calculation of the Ekman drift. In the HR simulation model, the Ekman drift is calculated at the surface, using a constant Ekman depth and a 45° deviation angle with the wind vectors. In the LR simulation model, the OSCAR data set provides Ekman currents by averaging Ekman currents within the 30 m surface layer. Comparisons between OSCAR product and current measurements from drifters to ADCP have been carried out by Johnson et al. (2007). They reported that the OSCAR calculation poorly reproduces the variability of the meridian component of the velocity and underestimates its magnitude.

FMD drift deduced from the HR mesoscale filtered field shows a similar trend as the ones deduced from the HR total and HR Ekman surface currents (Fig. 3a, respectively, the thin line with vertical bars melted with the thick line and the thick dashed line). The influence of the mesoscale activity induced by geostrophy is highlighted by the eastward advection of FMD along the STCC, which appears to be longer than in the HR simulation (Fig. 3b and c, thin line with vertical bars). Weakening the impact of geostrophic induced eddies also decreases the latitudinal dispersion of FMD in the convergence zone (figure not shown) which suggests a shift

from a geostrophic to an Ekman predominant regime in the convergence zone. From the Australian coast to the eastern-centre of the gyre, FMD gathered roughly along 30°S, which is a pattern highlighted in the HR Ekman simulation (figure not shown).

#### 3.5. Interannual variability

The interannual variability is investigated from the HR total surface current field through 2 year simulations, starting each month of January from 1993 to 1999 on a 1/3° initial sampling grid. During the first two years, as presented in Section 3.3, the convergence process toward [20°S; 40°S] is mainly driven by the Ekman drift. Therefore, it is not surprising to notice that in 1997, during the strong El Niño event, there is a decrease in FMD density in the convergence zone (Fig. 5a 1st year thick line and 2nd year thin line with vertical bars) due to a weakening or reverse of the equatorial winds (Delcroix, 1998; McPhaden, 1999; Picaut et al., 2001). Similarly in 1998, when the winds, and so Ekman drift, strengthened during La Niña event, there is an increase of FMD density in the convergence zone (Fig. 5a 1st year thick dashed line and 2nd year thick line). These two patterns are emphasized in the western part of the convergence zone (Fig. 5b) compared to the eastern part (Fig. 5c).

However, although interannual variations governed by surface oceanic circulation occur, the long-term trends remain similar.

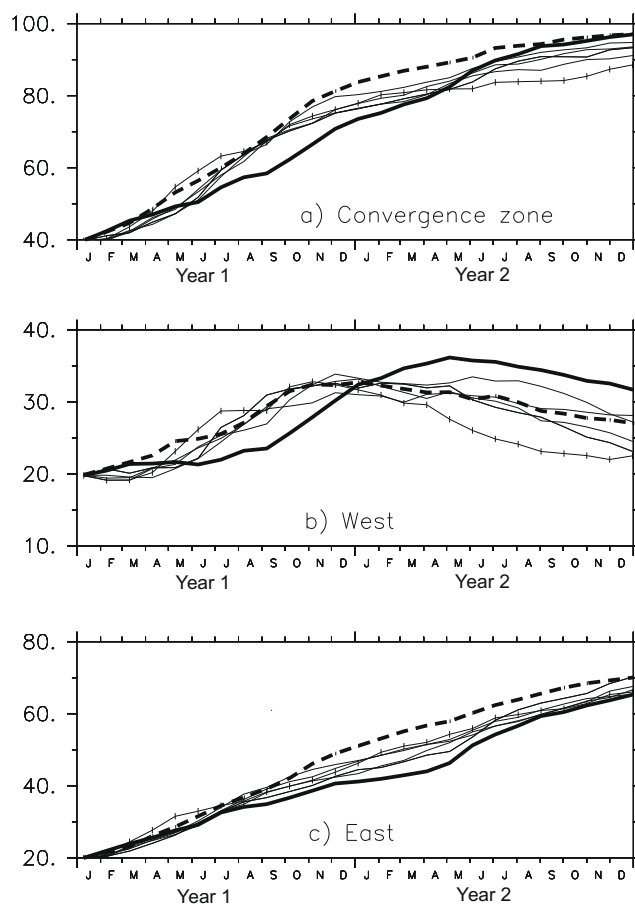


Fig. 5. Marine debris density (in%) during the first two years of their drift in: (a) the convergence zone, (b) its western part and (c) its eastern part. Particles are released every January from 1993 to 1999 (thin line). Results from the simulation initiated in 1996 (thin line with vertical bars), 1997 (thick line) and 1998 (thick dashed line) are indicated.

### 3.6. Debris of coastal origins

Most manmade floating pollution originates from coasts to islands. Fig. 6 shows the position of FMD, issued from the HR total surface current field as in Section 3.2, according to their initial locations around the coasts of South America, Australia and Tasmania, New Zealand, French Polynesia, New Caledonia and Fiji.

Most of FMD released from the South America near shore directly drift to the accumulation area within two years (Fig. 6a), while part of the debris is trapped in the near shore current systems where they stay along the coast of Chile. This latter result, consistent with recent reports by Thiel et al. (2003), draws back our attention to the permanence of marine debris on shores. As illustrated on Fig. 6, wherever the coastal regions FMD are released from, some of them not only runs aground on close but also remote shores.

For instance, in the western Pacific, the SEC bifurcates at the Australian coast as one part is flowing southward to become the EAC and the other part is flowing northward via the North Queensland Current into the Solomon Sea (Qu and Lindstrom, 2002; Kessler and Gourdeau, 2007). Therefore, some of the particles drifting from tropical Pacific archipelagos (Fig. 6b and c) reach coastal areas

from Fiji islands to Australia, as well as northward close to the equator in Papua New Guinea, or southward around 35°S in New Zealand. On the other hand, most of FMD released in the centre of the South Pacific around French Polynesian archipelagos (Fig. 6b) have reached the accumulation area after 8 years, while a small amount is still drifting in the STCC. When FMD originate from farther west, around New Caledonia and Fiji Islands (Fig. 6c), a larger amount is still drifting in the convergence zone after 8 years due to the longer distance to cover along the STCC before reaching the accumulation area.

FMD released close to the East Australian coast (Fig. 6d) and New Zealand (Fig. 6e) show a similar trend: the farther they are from the accumulation area, the longer they have to drift along the STCC and the more numerous they are in the convergence zone at the end of the simulation. Some of them are also trapped all along the coasts where they are released from.

### 4. Summary and discussion

The fate of the floating marine debris in the South Pacific Ocean has been addressed by considering their drift along surface currents. The surface currents are determined with an unprecedented

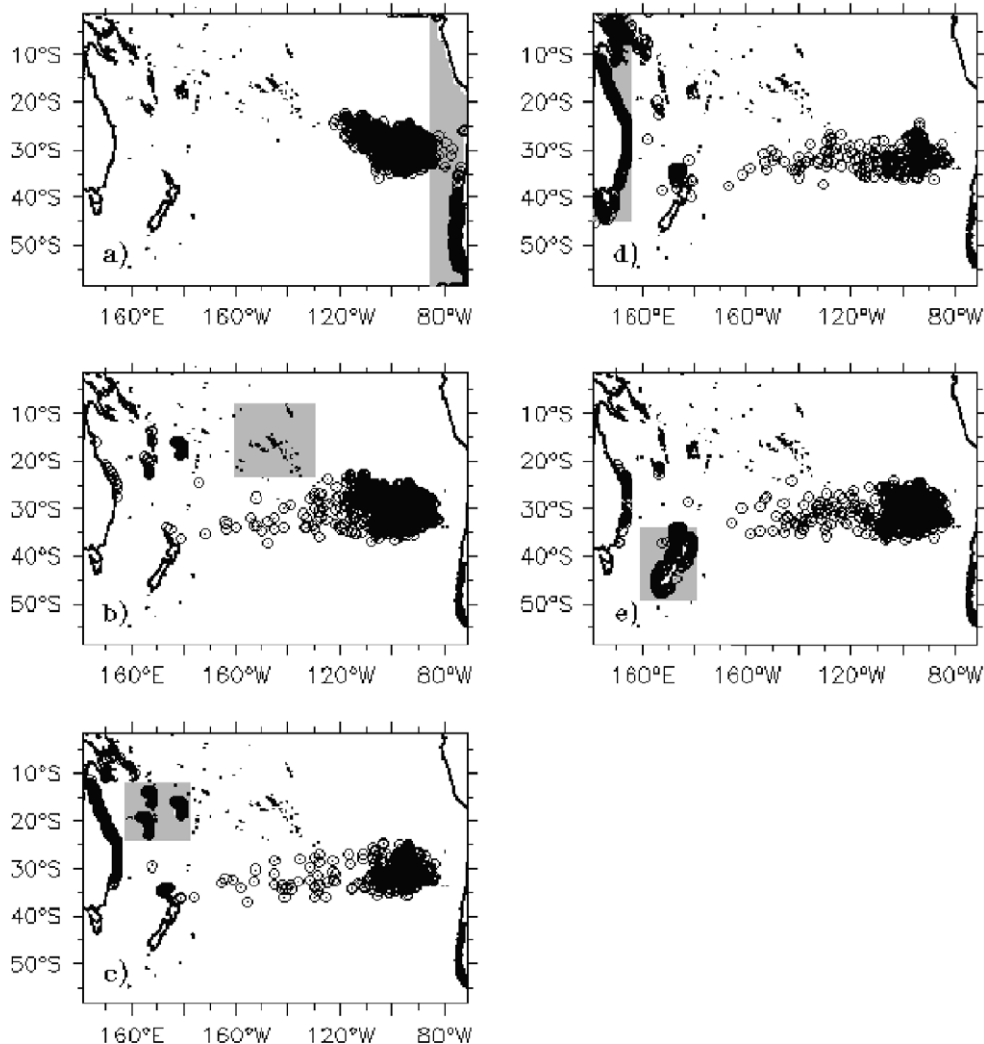


Fig. 6. Drift trajectories in the South Pacific with departure from (a) the western coast of South America, (b) French Polynesia, (c) New Caledonia and Fiji, (d) Australia and Tasmania, (e) New Zealand. Both initial (grey filled square) and final positions (black circles) of debris are indicated.

high resolution ( $1/3^\circ$  grid every 7 days) and high accuracy data. The drift of FMD is deduced by processing their dispersion from homogeneous distribution over a maximum time window of eight years. Our results show that the drift mechanism of surface marine debris consists in a three-step process: first, the marine debris drift to the tropical convergence zone between  $20^\circ\text{S}$  and  $40^\circ\text{S}$  due to the Ekman drift; second, they are transported eastward by the geostrophic currents; third, they accumulate and remain in the eastern-centre region of the subtropical gyre. This study shows the complementary role of the Ekman drift and the geostrophic drift, and the appropriateness of using a high resolution geostrophic field regarding the impact of mesoscale activity on FMD drift. It also shows for the first time after a long-term drift that all debris reaching the eastern-centre region of the subtropical gyre could not leave the region anymore. Oceanic circulation interannual variability, such as the strong 1997–1999 ENSO event, does not modify on a large scale the drift mechanism proposed above. It is also noteworthy that a large amount of marine debris released from islands to coastal regions, which we expect to be the main source of detritus, are discharged toward the open ocean while some of them are trapped by near shore current systems where they stay or run aground.

Trajectories of floating marine debris have been studied over a shorter time period in the North Pacific Ocean by Kubota et al. (2005). Their study showed that a significant amount of floating matter accumulates east of  $210^\circ\text{E}$  in a north–south direction, along the western and northern boundaries. The differences in the accu-

mulation systems between the North Pacific Ocean and the South Pacific Ocean are due to the distribution of the winds and the strong western boundary (Kuroshio) current in the North Pacific Ocean. In the South Pacific, our results demonstrate that after a longer time period of drift, FMD accumulates in the eastern-centre region of the subtropical gyre from where they do not escape. This observation is in agreement with Maximenko (2006) analysis of drifter trajectories. Fig. 7 shows the 57 drifter trajectories in the eastern-centre region of the subtropical gyre of the South Pacific Ocean. Maximenko (2006) shows that in all ocean basins except the South Pacific Ocean drifters trapped in the centre of the gyre can leave this region. According to his conclusion, this particularity of the South Pacific is due to the wind steadiness. Our study confirms the importance of the Ekman drift in maintaining the FMD in the centre of the gyre.

The Ekman currents are calculated assuming a deflected left angle of  $45^\circ$  between the surface wind vectors and the Ekman current vectors. Maximenko et al. (2004) investigated the variability of this angle according to the latitude and seasons using altimetric sea level heights and anomalies, wind data and drifters. Comparison of our results and their streamlines at 15 m depth shows differences (see Fig. 2 from Maximenko and Niiler, 2005) which were expected to be due to the weakening and direction changes of the Ekman spiral with depth, in particular at mid-latitudes. However, what has to be considered is the similarity between their flow field large scales patterns and ours, and adapting the deflected angle would not change much our solution on a long time-scale since only the

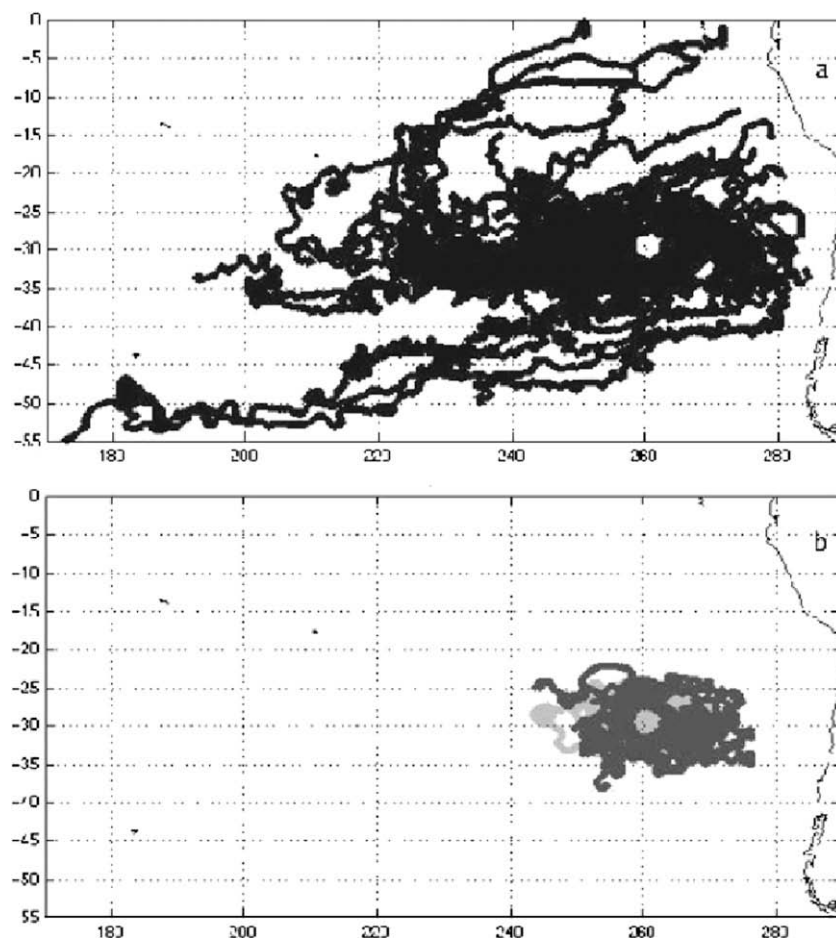


**Fig. 7.** (a) Trajectories of 57 drifters before entering the white circle in the centre of the gyre. (b) Dark grey are parts of trajectories after leaving from the circle and grey are parts of trajectories leaving from the circle and returning back into the circle again (courtesy to Maximenko (2006)).

curvature of the streamlines is modified. Our simulation with the OSCAR data shows discrepancies with our results due to the Ekman drift. Our analysis follows Johnson et al. (2007) results which show that the variability in the meridian component of the Ekman drift calculated from the OSCAR data set is underestimated.

After considering FMD drift from a physical point of view (as passive tracers following surface currents and physical dynamics), we consider the ecological aspects. It is worrying to notice that although population is aware of the visible part of the pollution, the one we are directly confronted to on beaches, we forget and barely care about the tremendous amount of detritus discharged in the open ocean. With about less than a decade for FMD to reach the accumulation area and a lifetime often longer than ten years (such as plastic bags), we should wonder what happens to those accumulated detritus. As the horizontal convergence upper layer induces a vertical divergence in the lower layer, are some of the dislocated plastic fragments trapped? Do they sink? Do they accumulate in the sediments at the bottom of the oceans?

It is difficult to estimate the damages in the eastern-centre region of the subtropical gyre since there is only one island, Easter Island, and no surveys carried out in the region. However, considering the increasing number of observations in the North Pacific reporting an extraordinarily high densities of derelict fishing gear and anthropogenic debris in the Northwestern Hawaiian Islands and the more populated main Hawaiian Islands (Kubota, 1994; Donohue et al., 2001; Boland and Donohue, 2003; Pichel et al., 2003), people should worry about the same happening in the South Pacific Ocean, and care should be brought regarding the increasing plastic products and other detritus that are released by our polluting way of life.

## Acknowledgments

Discussions and comments from Drs. N. Maximenko and K. Richards have been greatly appreciated. Insightful comments of the reviewer greatly helped improve the manuscript. Thanks to Diane Henderson for helpful corrections. E.M. was supported by a grant from the Research Ministry of French Polynesia.

## References

- Boland, R.C., Donohue, M.J., 2003. Marine debris accumulation in the nearshore marine habitat of the endangered Hawaiian monk seal, *Monachus schauinslandi* 1999–2001. *Marine Pollution Bulletin* 46, 1385–1394.
- Bonjean, F., Lagerloef, G.S.E., 2002. Diagnostic model and analysis of the surface currents in the tropical Pacific Ocean. *Journal of Physical Oceanography* 32, 2938–2954.
- Chaigneau, A., Pizarro, O., 2005. Mean surface circulation and mesoscale turbulent flow characteristics in the eastern South Pacific from satellite tracked drifters. *Journal of Geophysical Research* 110 (C6), C05014.
- Chen, D., Liu, W.T., Zebiak, S.E., Cane, M.A., Kushnir, Y., Witter, N.D., 1999. Sensitivity of the tropical Pacific Ocean simulation to the temporal and spatial resolution of wind forcing. *Journal of Geophysical Research* 104 (C5), 11261–11272.
- Delcroix, T., 1998. Observed surface oceanic and atmospheric variability in the tropical Pacific at seasonal and ENSO timescales: a tentative overview. *Journal of Geophysical Research* 103 (C9), 18,611–18,634.
- Donohue, M.J., Boland, R.C., Sramek, C.M., Antonelis, G.A., 2001. Derelict fishing gear in the Northwestern Hawaiian Islands: diving surveys and debris removal confirm threat to coral reef ecosystems. *Marine Pollution Bulletin* 42 (12), 1301–1312.
- Ducet, N., Le Traon, P.Y., 2001. A comparison of surface Eddy kinetic energy and Reynolds stress in the Gulf Stream and the Kuroshio current systems from merged Topex/Poseidon and ERS-1/2 altimetric data. *Journal of Geophysical Research* 106 (C8), 16603–16622.
- Fu, L.L., Christensen, E.J., Yamarone Jr., C.A., Lefebvre, M., Menard, Y., Dorner, M., Escudier, P., 1994. Topex/Poseidon mission overview. *Journal of Geophysical Research* 99 (C12), 24369–24381.
- Gregory, M.R., 1978. Accumulation and distribution of virgin plastic granules on New Zealand beaches. *New Zealand Journal of Marine and Freshwater Research* 12, 399–414.
- Gregory, M.R., Ryan, P.G., 1997. Pelagic plastics and other seaborne persistent synthetic debris: a review of Southern hemisphere perspectives. In: Coe, J.M., Rogers, D.B. (Eds.), *Marine Debris—Sources*.
- Jakobsen, P.K., Ribergaard, M.H., Quadfasel, D., Scmith, T., Hughes, C.W., 2003. Near surface circulation in the northern North Atlantic as inferred from Lagrangian drifters: variability from the mesoscale to interannual. *Journal of Geophysical Research* 108 (C8), 16603–16622.
- Jingzhi, S., Mingkui, L., Yijun, H., Baoshu, Y., Guohong, F., 2006. Surface circulation derived from drifting buoys in mid-and low-latitude Pacific. *Chinese Journal of Oceanology and Limnology* 24 (4), 333–337.
- Johnson, E.S., Bonjean, F., Lagerloef, G.S.E., Gunn, J.T., Mitchum, G.T., 2007. Validation and error analysis of OSCAR Sea surface currents. *Journal of Atmospheric and Oceanic Technology* 24, 688–701.
- Kessler, W.S., Gourdeau, L., 2007. The annual cycle of circulation of the southwest subtropical Pacific, analyzed in an ocean GCM. *Journal of Physical Oceanography* 37, 1610–1627.
- Klinck, J.M., Nowlin Jr., W.D., 2001. Antarctic circumpolar current. *Encyclopedia of Ocean Science*, first ed. Academic Press, New York, pp. 151–59.
- Kubota, M., 1994. A mechanism for the accumulation of floating marine debris north of Hawaii. *Journal of Physical Oceanography* 5, 1059–1064.
- Kubota, M., Takayama, K., Namimoto, D., 2005. Pleading for the use of biodegradable polymers in favor of marine environments and to avoid an asbestos-like problem for the future. *Applied Microbiology and Biotechnology* 67 (4), 469–476.
- Lagerloef, G.S.E., Mitchum, G., Lukas, R.B., Niiler, P.P., 1999. Tropical Pacific near-surface currents estimated from altimeter, wind, and drifter data. *Journal of Geophysical Research* 104 (C10), 23,313–23,326.
- Le Traon, P.Y., Nadal, F., Ducet, N., 2003. An improved mapping method of multisatellite altimeter data. *Journal of Atmospheric and Oceanic Technology* 15, 522–533.
- Levitus, S., Monterey, G.L., Boyer, T., 1992. Seasonal variability of dynamic height and its Fourier analysis. Available from: <<http://www.nodc.noaa.gov/OC5/dyn.html>>.
- McPhaden, M.J., 1999. Genesis and evolution of the 1997–98 El Niño. *Science* 283, 950–954.
- Martinez, E., Maamaatuaiahutapu, K., Payri, C., Ganachaud, A., 2007. *Turbinaria ornata* invasion in the Tuamotu Archipelago, French Polynesia: ocean drift connectivity. *Coral Reefs* 26 (1).
- Martins, C.S., Hamann, M., Fiuza, A.F.G., 2002. Surface circulation in the eastern North Atlantic, from drifters and altimetry. *Journal of Geophysical Research* 107 (C12), 3217.
- Mata, M.M., Tomczak, M., Wijffels, S., Church, J.A., 2000. East Australian current volume transports at 30°S: estimates from the World Ocean circulation experiment hydrographic sections PR11/P6 and the PCM3 current meter array. *Journal of Geophysical Research* 105 (C12), 128509.
- Maximenko, N.A., 2006. Multi-scale aspects of oceanic circulation. In: Presentation at the Sixth IPRC Symposium, Honolulu, Hawaii, May 8–9.
- Maximenko, N.A., Niiler, P.P., 2005. Hybrid decade-mean global sea level with meso-scale resolution. In: Saxena, N. (Ed.), *Recent Advances in Marine Science and Technology*. PACON International, Honolulu, pp. 55–59.
- Maximenko, N.A., Niiler, P.P., Cornuelle, B., Kim, Y.Y., Liu, W.T., 2004. The dynamics of ocean surface circulation studied using altimeter, Lagrangian drifter and wind data. In: *NASA Ocean Surface Topography Science Team Meeting*, St Petersburg, Florida, USA, November 4–6.
- Merle, J., Rotschi, H., Voituriez, B., 1969. Zonal circulation in the tropical western South Pacific at 170°E. *Bulletin of Japanese Society Fisheries Oceanography*, 91–98. Special Issue (Prof. Uda's Commemorative Papers).
- Morris, M., Roemmich, D., Cornuelle, B., 1996. Observations of variability in the South Pacific subtropical gyre. *Journal of Physical Oceanography* 26 (11), 2359–2380.
- Picaut, J., Ioualalen, M., Delcroix, T., Masia, F., Murtugudde, R., Vialard, J., 2001. The oceanic zone of convergence on the eastern edge of the Pacific warm pool: a synthesis of results and implications for El Niño Southern Oscillation and biogeochemical phenomena. *Journal of Geophysical Research* 106 (C2), 2363–2386. doi:10.148-0227/01/2000JC900141.
- Pichel, W.G., Veenstra, T., Churnside, J., Arabini, E., Friedman, K.S., Foley, D., Brainard, R., Kiefer, D., Ogle, S., Clemente-Colon, P., 2003. Ghost net-derelict net detection in the North Pacific and Alaska waters using satellite and airborne remote sensing and surface drifters. In: *Proceedings of the Thirtieth International Symposium on Remote Sensing of the Environment*, Honolulu, USA.
- Pond, S., Pickard, G.L., 1983. *Introductory Dynamical Oceanography* (2nd ed.).
- Qiu, B., Chen, S., 2004. Seasonal modulations in the Eddy field of the South Pacific Ocean. *Journal of Physical Oceanography* 34 (7), 1515–1527.
- Qu, T., Lindstrom, E.J., 2002. A climatological interpretation of the circulation in the western South Pacific. *Journal of Physical Oceanography* 32, 2492–2508.
- Ryan, P.G., Moloney, C.L., 1993. Marine litter keeps increasing. *Nature* 361, 23.
- Stammer, D., Wunsch, C., 1994. Preliminary assessment of the accuracy and precision of Topex/Poseidon altimeter data with respect to the large-scale circulation. *Journal of Geophysical Research* 99 (12), 24584–24604.
- Stamma, L., Peterson, R.G., Tomczak, M., 1995. The South Pacific current. *Journal of Physical Oceanography* 77, 91.
- Taillandier, V., Griffa, A., Molcard, A., 2006. A variational approach for the reconstruction of regional scale Eulerian velocity fields from Lagrangian data. *Ocean Modelling* 13, 1–24.
- Thiel, M., Hinojosa, I., Vasquez, N., Macaya, E., 2003. Floating marine debris in coastal waters of the SE-Pacific (Chile). *Marine Pollution Bulletin* 46, 224–231.

Wakata, Y., Sugimori, Y., 1990. Lagrangian motions and global density distributions of floating matter in the ocean simulated using shipdrift data. *Journal of Physical Oceanography* 20 (1), 15–28.

Wilks, S., 2006. The plastic baggers, an evaluation of a boutique cause in targeted environmentalism. *Australian Quarterly* 78.